Nanotextured polymer substrates show enhanced cancer cell isolation and cell culture

2015 Nanotechnology 26 225101

(http://iopscience.iop.org/0957-4484/26/22/225101)

IOP Publishing Nanotechnology
Nanotechnology 26 (2015) 225101 (9pp) doi:10.1088/0957-4484/26/22/225101

Nanotextured polymer substrates show enhanced cancer cell isolation and cell culture

Muhymin Islam[1,2,3], Adeel Sajid[1,3,4,5], M Arif Iftakher Mahmood[1,2,3], Mohammad Motasim Bellah[1,2,3], Peter B Allen[6], Young-Tae Kim[3,7,8] and Samir M Iqbal[1,2,3,7,8]

[1] Nano-Bio Lab, University of Texas at Arlington, Arlington, TX 76019, USA
[2] Department of Electrical Engineering, University of Texas at Arlington, Arlington, TX 76011, USA
[3] Nanotechnology Research Center, University of Texas at Arlington, Arlington, TX 76019, USA
[4] Interdisciplinary Studies Program, Department of Biology, University of Texas at Arlington, Arlington, TX 76019, USA
[5] Department of Biology, University of Texas at Arlington, Arlington, TX 76019, USA
[6] Department of Chemistry, University of Idaho, Moscow, ID 83844-2343, USA
[7] Department of Bioengineering, University of Texas at Arlington, Arlington, TX 76010, USA
[8] Department of Urology, University of Texas Southwestern Medical Center at Dallas, Dallas, Texas, 75390, USA

E-mail: SMIQBAL@uta.edu

Received 23 November 2014, revised 28 February 2015
Accepted for publication 11 March 2015
Published 11 May 2015

Abstract

Detection of circulating tumor cells (CTCs) in the early stages of cancer is a great challenge because of their exceedingly small concentration. There are only a few approaches sensitive enough to differentiate tumor cells from the plethora of other cells in a sample like blood. In order to detect CTCs, several antibodies and aptamers have already shown high affinity. Nanotexture can be used to mimic basement membrane to further enhance this affinity. This article reports an approach to fabricate nanotextured polydimethylsiloxane (PDMS) substrates using micro reactive ion etching (micro-RIE). Three recipes were used to prepare nanotextured PDMS using oxygen and carbon tetrafluoride. Micro-RIE provided better control on surface properties. Nanotexturing improved the affinity of PDMS surfaces to capture cancer cells using surface immobilized aptamers against cell membrane overexpressed with epidermal growth factor receptors. In all cases, nanotexture of PDMS increased the effective surface area by creating nanoscale roughness on the surface. Nanotexture also enhanced the growth rate of cultured cells compared to plain surfaces. A comparison among the three nanotextured surfaces demonstrated an almost linear relationship between the surface roughness and density of captured tumor cells. The nanotextured PDMS mimicked biophysical environments for cells to grow faster. This can have many implications in microfluidic platforms used for cell handling.

Keywords: RNA aptamers, nanotextured substrates, reactive ion etching, PDMS, microfluidics, human glioblastoma, basement membrane

(Some figures may appear in colour only in the online journal)

1. Introduction

Several strategies have been reported to detect and isolate cancer cells at early stages, but these are limited by yield, cost and purity [1–10]. Early detection results in effective therapy and can significantly reduce the cancer-related mortality rate [11, 12]. Affinity interaction based detection and sorting, especially with aptamers, can provide high specificity and

selectivity [13, 14]. Epidermal growth factor receptor (EGFR) specific RNA aptamer functionalized substrates have been shown to recognize, capture and isolate human glioblastoma (hGBM) cells with high specificity [15, 16].

Several other studies have demonstrated that cell capture, growth, adhesion and orientation are influenced by nanoscale topography of the functionalized surfaces [16–19]. In tissue engineering, some studies have shown that nanostructured scaffolds can significantly increase the densities of certain cells [20, 21]. The key feature of a nanotextured surface is the increased surface area to capture a larger number of probe antibodies or nucleic acids [16, 18, 22, 23]. Some applications of nanotextured surfaces are found in biosensors, proteomics and light emitting diodes as well [24–28]. Nanotextured surfaces can be prepared using processes like micro-contact printing, stencil assisted patterning or long polymer chemical etching. These processes are time consuming and cost prohibitive [16, 17, 29]. Several studies have also reported plasma etching to prepare nanotextured surfaces [22, 23, 30].

Polydimethylsiloxane (PDMS) is a widely used polymer in biomedical research due to its stable chemical and physical properties [31]. A simple way to prepare three-dimensional, nanotextured PDMS substrates and their applications to isolate, enrich and culture tumor cells are reported here. Micro-reactive ion etching (micro-RIE) was performed to create nanotexture on PDMS substrates. These substrates were functionalized with anti-EGFR aptamer for cell isolation. It was seen that the nanoscale topography of PDMS increased the affinity of cancer cell attachment by providing a larger surface area for aptamer immobilization. The increased surface area allowed a higher number of available aptamer copies on the surface to capture cells. The nanotextured surfaces also showed higher cell growth: the growth rate for tumor cells was as high as the growth rates in the standard well plates used for cell culture. Furthermore, the comparison of three nanotextured surfaces showed almost linear relationships for both cell capture and cell growth with respect to surface roughness. The nanotexture enhanced cell capture probability and growth rate, both of which are very important for microdevices used for detecting and enriching rare cells. The key findings showed that nanotexture of the substrate could be quantitatively controlled to tweak the density of available ligands for possible match with the overexpression of oncogenes. This can possibly lead to nanotextured PDMS devices that can also stage cancer cells based on overexpression.

2. Materials and methods

All chemicals were obtained from Sigma-Aldrich (St. Louis, MO) unless noted otherwise.

2.1. Aptamer preparation

Aptamer was prepared using a standard procedure reported earlier [16]. For anti-EGFR RNA aptamer selection with SELEX process, purified human EGFR (R&D Systems, Minneapolis, MN) was used. The anti-EGFR aptamers ($K_d = 2.4$ nM) were extended with a capture sequence. The amine-modified capture probe was used to immobilize aptamers on the substrates through duplex formation. The sequences of the extended anti-EGFR aptamers and substrate-anchored capture molecules were: anti-EGFR aptamer, 5′-GGC GCU CCG ACC UUA GUC UCU GUG CCG CUA UAA UGC ACG GAU UUA AUC GCC GUA GAA AAG CAU GUC AAA GCC GGA ACC GUG UAG CAC AGC AGA GAA UUA AAU GCC CGC CAU GAC CAG-3′ and substrate anchored capture DNA, 5′-amine-CTG GTC ATG GCG GGC ATT TAA TTC-3′ [16].

2.2. Preparation of nanotextured PDMS substrates

PDMS was mixed (10:1, wt/wt) with Sylgard 184 silicone elastomer curing agent (Dow Corning) and degassed in a desiccator for 1 h to remove all air bubbles. PDMS was then poured on a 4 inch silicon wafer and heated to 75 °C for 5 min and then 150 °C for 10 min. Next, the PDMS was peeled off from the silicon substrate and cut into small pieces ($\sim 2 \times \sim 2$ inch^2). These substrates were cleaned in isopropyl alcohol (IPA), rinsed in deionized (DI) water and dried in nitrogen. A reactive ion etch (RIE) series 800 plasma system was used to prepare nanotextured PDMS. Three recipes were used in this system to etch the PDMS using mixture of oxygen (O_2) and carbon tetrafluoride (CF_4). First of all, the etching was performed with two ratios of etchant gases for a specific time of 12 min. In recipe 1, the flow rate of O_2 and CF_4 was 10 sccm, respectively (ratio of O_2:CF_4 was 1:1) and in recipe 2, the flow rate of O_2 and CF_4 was 7 sccm and 14 sccm, respectively (ratio of O_2:CF_4 was 1:2). In recipe 3, the flow rate of gases was the same as in recipe 1, but the etching time was increased to 25 min. After etching, each substrate was cleaned in sonicated IPA followed by cleaning in piranha solution (H_2O_2:H_2SO_4, 1:3). In the remaining article, the three PDMS surfaces prepared by recipes 1, 2 and 3 will be named as Surface-1, Surface-2 and Surface-3, respectively.

2.3. Surface characterization

Surface topography of PDMS surfaces was evaluated quantitatively with a Dimension 5000 atomic force microscope (AFM). The root mean square surface roughness was measured. Micrographs of PDMS samples were captured in the ambient air with 15–20% humidity at a tapping frequency of approximately 300 kHz [16]. The analyzed field measured $10 \times 10\ \mu m^2$ at a scan rate of 1 Hz with 256 scanning lines.

2.4. Elemental composition of the samples

Energy dispersive x-ray spectroscopy (EDS) was used for elemental analysis of plain and nanotextured PDMS. All samples were coated with a thin layer of silver (Ag) before this analysis. Here, an EDS detector (EDAX, Genesis) was attached to the scanning electron microscope (SEM). The SEM was focused at a 15 mm working distance with 20 kV accelerating voltage and data recording was followed by a mapping analysis.

2.5. Contact angle measurements

Contact angles for plain and nanotextured PDMS substrates were measured using a contact angle goniometer (NRL-100; Rame-Hart, Washington, DC). On average, five measurements were taken for each run. Angles were measured twice for each substrate. First, the angles were measured on substrates without any modification and next on substrates functionalized by isothiocyanate.

2.6. Attachment of anti-EGFR aptamer on PDMS substrates

The aptamer attachment was adapted from our previous work [16]. PDMS substrates were cut into $10 \times 10\ \text{mm}^2$ pieces. These small pieces were cleaned with UV–ozone plasma for 30 min followed by piranha solution dip. These substrates were then rinsed with DI water and dried in nitrogen flow and immersed in 3% (v/v) of (3-aminopropyl)triethoxysilane (APTES) in methanol for 30 min at room temperature. Next, the substrates were washed in DI water and methanol; and cured for 30 min at 120 °C. Substrates were then put in dimethylformamide (DMF) for 5 h at 45 °C. DMF had 10% pyridine and 1 mmol/l*p*-phenylene diisothiocyanate (PDITC) in it. After 5 h, substrates were rinsed with DMF and 1,2-dichloroethane and dried in nitrogen gas. A $30\ \mu\text{mol l}^{-1}$ concentration of capture DNA (which had a 5′ amine group) was prepared using DI water with 1% *N,N*-diisopropylethylamine (DIPEA) and the substrates were incubated in the DNA solution overnight in a humid chamber at 37 °C. After incubation, the substrates were washed with methanol and diethylpyrocarbonate (DEPC) treated DI water. Next, the substrates were immersed for 5 h in $150\ \text{mmol l}^{-1}$ DIPEA in DMF and $50\ \text{mmol l}^{-1}$ 6-amino-1-hexanol and again washed in ethanol, DMF, and DEPC-treated DI water. A glass chamber was then properly washed with RNase free and DEPC treated DI water and PDMS substrates were placed in it. Anti-EGFR RNA aptamer ($1\ \mu\text{mol l}^{-1}$) dissolved in 1X annealing buffer ($10\ \text{mmol l}^{-1}$ Tris (pH 8.0), $1\ \text{mmol l}^{-1}$ EDTA (pH 8.0), $1\ \text{mmol l}^{-1}$ NaCl) was placed on each substrate. After 2 h of incubation at 37 °C, substrates were washed with 1X annealing buffer and DEPC-treated DI water for 5 min. 1X PBS (pH 7.5) with $5\ \text{mmol l}^{-1}$ magnesium chloride solution was prepared and the substrates were then placed in it before being used for experiments. The experiments were run within a few hours of functionalization.

2.7. Fluorescence measurements

Surface modification was confirmed by fluorescence measurements of acridin orange (AO) stain. DNA attached PDMS surfaces were used to measure the intensity of AO. An AO solution of $2\ \text{mg ml}^{-1}$ concentration was prepared in sterilized DI water. DNA functionalized plain and nanotextured PDMS surfaces were completely immersed into the solution and kept on a shaker for 30 min. Then all samples were washed thoroughly in DI water and fluorescence measurements were taken at 480 nm wavelength using a Zeiss confocal microscope. The fluorescence intensities were analyzed with *ImageJ* software (National Institutes of Health, Bethesda, Maryland, USA).

2.8. hGBM and astrocyte cell culture

The culture of hGBM cells has been reported before [16]. Briefly, these cells were cultured in chemically defined, serum-free Dulbecco's Modified Eagle's Medium (DMEM)/F-12 medium supplemented with $20\ \text{ng ml}^{-1}$ mouse EGF (from Peprotech, Rocky Hill, NJ), 1X B27 supplement (Invitrogen, Carlsbad, CA), 1 × insulin-transferrin-selenium-X (ITS-X, Invitrogen), and penicillin:streptomycin $100\ \text{U ml}^{-1}$: $100\ \mu\text{g ml}^{-1}$ (HyClone, Wilmington, DE) and plated at a density of 3×10^6 live cells per 60 mm plate. The hGBM cells were transduced with a lentivirus expressing mCherry fluorescent protein. Human astrocyte cells were obtained from consenting patients at the University of Texas Southwestern Medical Center at Dallas (TX, USA) with the approval of the Institutional Review Board. The collected human astrocyte cells were cultured in DMEM/F-12 (Cellgro, Mediatech Inc.) with 10% fetal bovine serum. Gentamycin and L-glutamine (Invitrogen) were added to the cell culture medium. Standard cell culture conditions i.e. a sterile, humidified, 95% air, 5% CO_2 and 37 °C were maintained to incubate cells.

2.9. Tumor and astrocyte cell capture on substrates

First, cell suspensions were centrifuged and the supernatants were removed. Next, 1X PBS solution (with 5 mM $MgCl_2$) was added to dilute the cells to a concentration of 100 000 cells ml^{-1}. Approximately 500 μl drop of cell suspension was put on each substrate and incubated for 30 min at 37 °C. After incubation, substrates were washed with sterilized 1X PBS on a shaker at 90 revolutions per minute for 15 min [16]. Then substrates were observed and micrographs were captured using Leica optical microscope. *ImageJ* was used to calculate cell density from captured micrographs. For each type of surface, eight and six samples were prepared for hGBM and astrocyte cells, respectively. The cell capture efficiency on surfaces was also calculated by taking the ratio of the total number of cells captured and the total number of cells suspended on each sample surface. Total number of cells captured on each sample was calculated from the cell density and total surface area of the samples. Statistical analysis was performed using one-way analysis of variance (ANOVA) for all types of surfaces.

2.10. In vitro cell culture studies on nanotextured PDMS

Fibroblasts, hGBM and human astrocyte cells were seeded on a standard well plate, plain PDMS and nanotextured PDMS substrates to observe the effects of nanotexturing on cell growth. All PDMS substrates were cut into 6 mm diameter circular disks, washed three times in DI water, dried in nitrogen flow and treated with O_2 plasma for 30 min. Next, the substrates were washed in 70% ethanol for 30 min to sterilize. Again, all substrates were washed with DI water three times and dried. The samples were then coated with

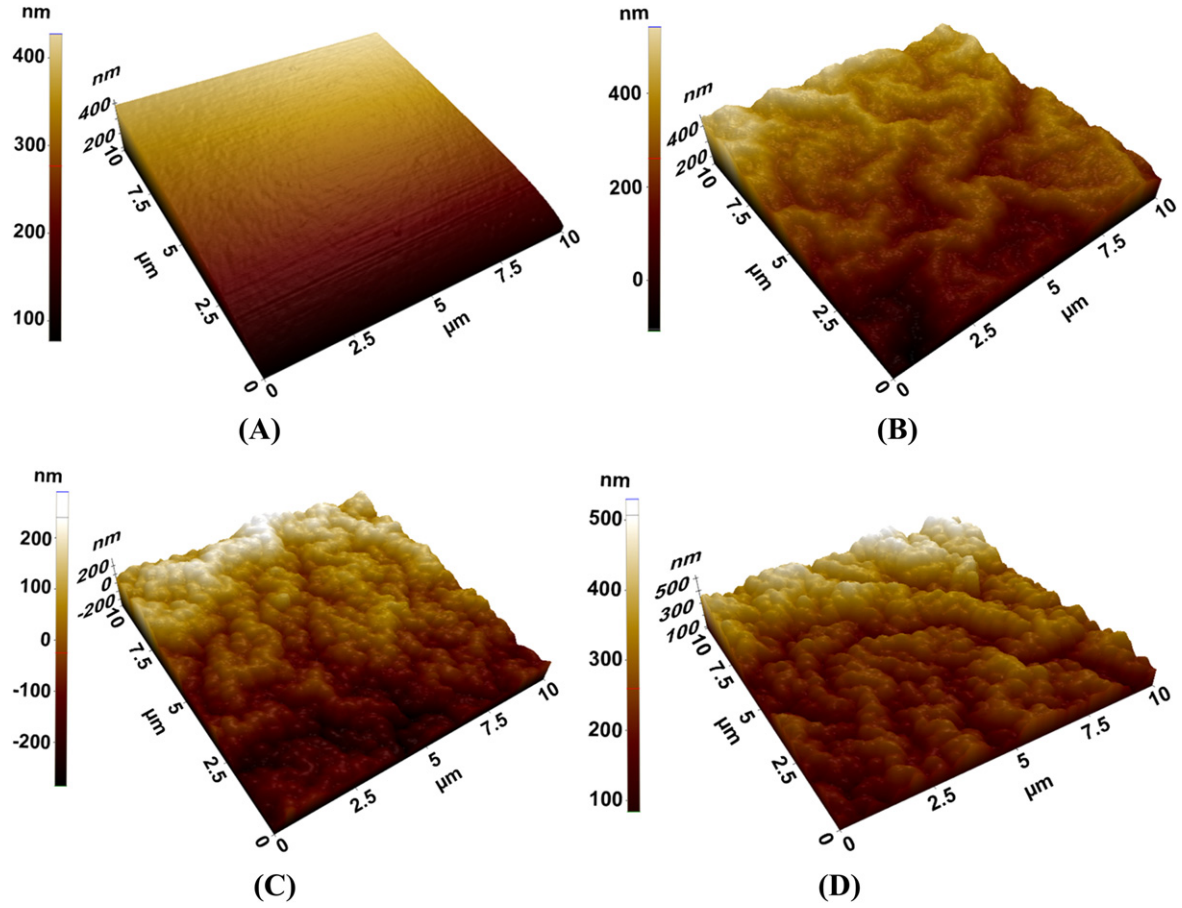

Figure 1. AFM micrographs of the plain and nanotextured PDMS surfaces. The micrographs show (A) plain PDMS surface; nanotextured PDMS surfaces obtained by micro-RIE using O_2 and CF_4, (B) after 12 min (O_2:CF_4, 1:1), (C) after 12 min (O_2:CF_4, 1:2), and (D) after 25 min (O_2:CF_4, 1:1).

poly-D-lysine (PDL) by immersing them in PDL solution for 24 h and then washed again in sterilized DI water thoroughly. The samples were then coated with laminin solution containing 10 μg ml^{-1} laminin in 1X PBS (PBS was Mg^{2+}/Ca^{2+} free) and incubated at 37 °C overnight to adhere laminin to the PDMS surfaces [18]. Next, samples were washed in sterilized 1X PBS and freshly harvested human fibroblasts, hGBM and human astrocyte cells were seeded (1000 cells ml^{-1}) onto the samples. The sample surfaces were observed under an optical microscope after three days. For each type of surface, five samples ($n = 5$) were prepared. Statistical analysis was also performed using one-way ANOVA for all types of surfaces.

3. Results and discussion

3.1. Surface topography of nanotextured substrates

The average measured roughness was 242.92 ± 87.71, 515 ± 102.28 and 629.17 ± 109.67 nm for Surface-1, Surface-2 and Surface-3, respectively (figure 1). From these numbers, it can be observed that a higher surface roughness was obtained when the ratio of CF_4 was higher than O_2. Similar feature was also achieved by using same amount of O_2 and CF_4 for a longer period of time. Therefore, it can be said that the features of nanotextured surfaces can be controlled by both the etch time and ratio of oxygen and carbon tetrafluoride. Moreover, this approach can be implemented to create nanotexture in microfluidic devices fabricated in PDMS. The devices will need to be fabricated first in PDMS and exposed to micro-RIE to create nanotexture. Several techniques use nanotextured templates to transfer patterns in PDMS [16, 17], but the presented approach does not need any template.

3.2. Elemental analysis and compositional mapping

PDMS is a polymer made of $SiOC_2H_6$ monomer. EDS elemental analysis of plain PDMS showed that it consisted of silicon, oxygen and carbon (figure 2(A)). Silver came from the coating. As hydrogen atom is very small with low atomic number, it could not be detected in EDS. Therefore, it was not found in the measurements. The EDS elemental analysis of nanotextured PDMS (Surface-3) showed almost identical results as native untreated PDMS (figure 2(B)). Therefore, it can be said that the etching did not influence the chemical nature of PDMS.

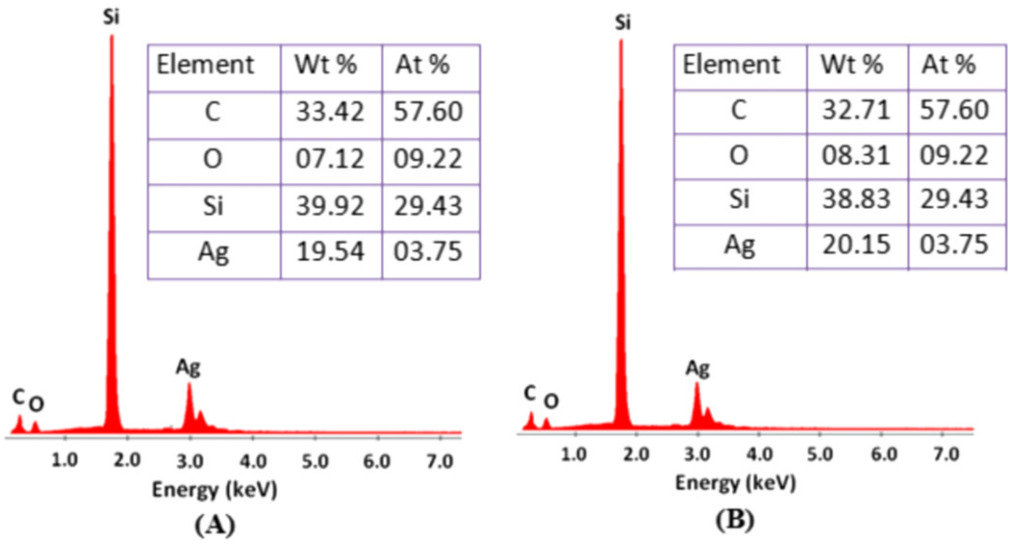

Figure 2. EDS elemental composition of (A) plain PDMS and (B) nanotextured PDMS (Surface-3).

3.3. Contact angle measurements

Contact angle from a water droplet gives the measurement of hydrophobicity or hydrophilicity of a surface [16]. Generally, the contact angle is more than 90° for hydrophobic surfaces, and less than 90° for hydrophilic surfaces. Due to nanotexturing, hydrophobicity increased for hydrophobic surfaces and hydrophilicity increased for hydrophilic surfaces [16, 23]. The contact angles of all experimental surfaces were measured and their average values with standard deviations are given in table 1. Without any modifications, all substrates were hydrophobic and after APTES and isothiocyanate functionalization, all substrates became hydrophilic.

Table 1. Contact angles measured on substrates after ultraviolet–ozone treatment and chemical activation with PDITC ($n = 5$).

Substrate type	Base substrate (°)	After PDITC treatment (°)
Flat PDMS	112.2 ± 2.77	66.2 ± 2.17
Surface-1	126.8 ± 3.11	56.2 ± 2.28
Surface-2	139.8 ± 2.39	52 ± 2.45
Surface-3	145.4 ± 2.19	48.4 ± 1.95

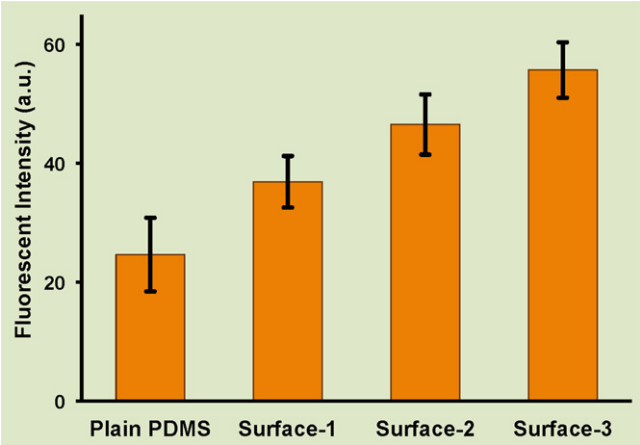

Figure 3. Fluorescence intensity from AO stain after DNA attachment on the substrates.

3.4. Fluorescence measurements

Proper hydrolysis of the PDMS surface after plasma treatment and piranha solution exposure significantly increased the number of available hydroxyl groups. This improved the number of available amino groups from adsorbed APTES. This in turn increased the number of DNA molecules attached and finally increased the total number of immobilized aptamers [16]. The relative number of DNA molecules on all substrates was determined by comparing relative fluorescence intensities of AO. The average fluorescence intensities of these substrates are given in figure 3. The signals from nanotextured PDMS substrates were higher compared to plain PDMS. The intensity was highest for Surface-3 and lowest for Surface-1. The nanotexture had an additional effect: it increased available surface area and consequently amplified the number of hydroxyl groups. Higher density of hydroxyl groups captured many more APTES molecules (with amino groups). This ultimately resulted in a higher number of immobilized DNA. Higher density of DNA was favorable in order to enhance the density of aptamer on the surface which led to better tumor cell isolation. The packing density of anchored DNA is a function of the radius of gyration of the molecules, and the radius of gyration defines the footprint of a molecule and density of packing [32]. Nanotextured surfaces reduced the distance between the immobilized ends of the probes as free ends had more room on curvaceous surfaces and thus required a smaller footprint compared to flat surfaces for the same radius of gyration [16]. Therefore, probe density was higher on curvaceous nanotextured surfaces. Again, nanotextured surfaces offered a higher effective area than plain surfaces of same areal size. As a result, the total number of captured molecules was increased and nonspecific aptamer adsorption was reduced on nanotextured surfaces. Non-

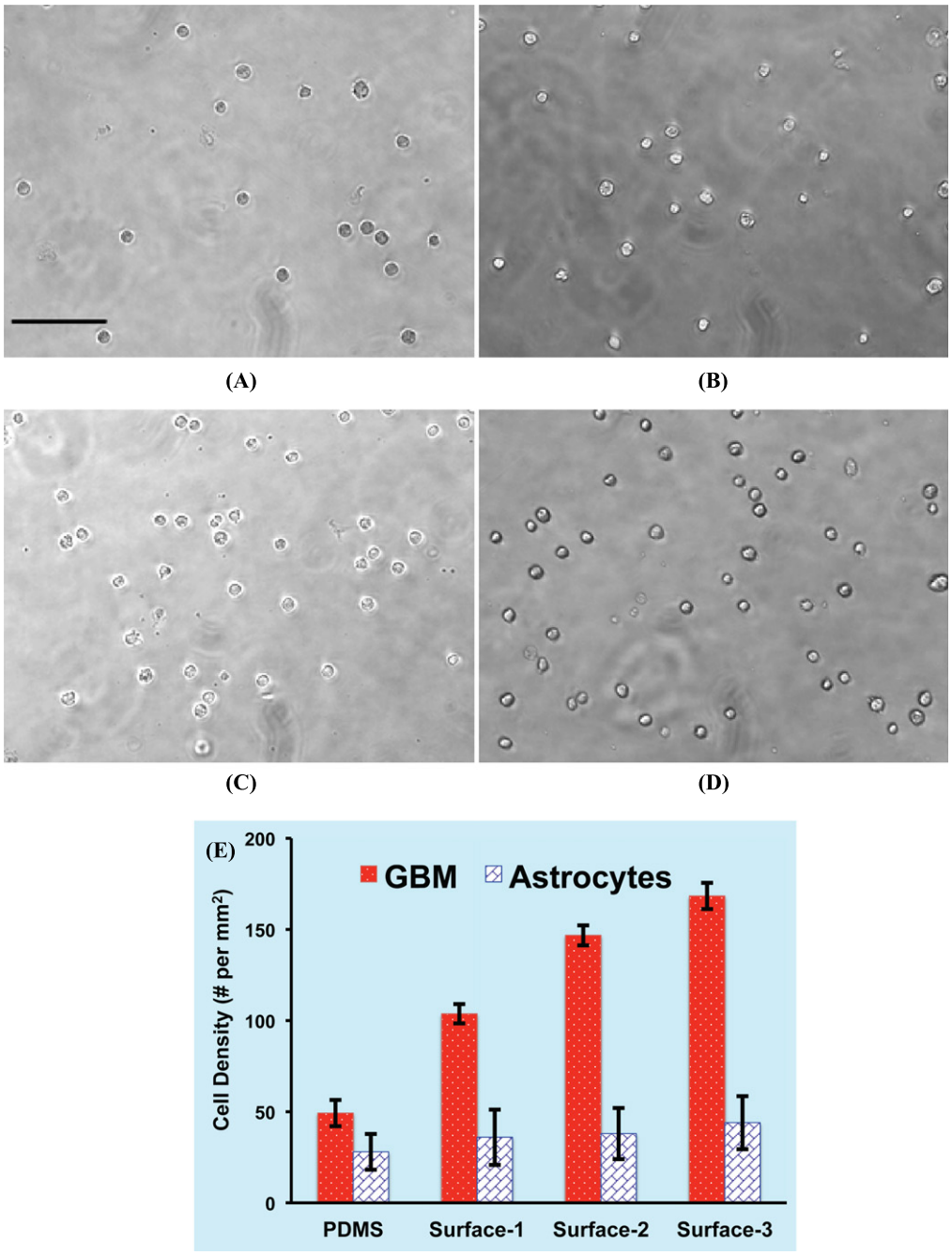

Figure 4. The hGBM cells on the anti-EGFR aptamer modified surfaces (A) plain PDMS surface; (B) Surface-1, (C) Surface-2 and (D) Surface-3; and (E) the average cell density (number of cells mm^{-2}) of hGBM and astrocytes cells on four surfaces. There were significant statistical differences for the density of hGBM cells among all surfaces with p-value <0.01 between any two surfaces ($n = 8$). Scale bar = 100 μm in (A) is also applicable for (B)–(D).

specific adsorption of aptamers occurred due to van der Waals forces only if aptamers could find their way to the surface. But the negative charge of tightly packed DNA repelled negatively-charged aptamers and reduced non-specific adsorption [16]. However, among the three nanotextured surfaces, fluorescence intensity was lowest for Surface-1. Surface-2 and Surface-3 showed higher intensity as they had higher surface roughness. Between these two surfaces, the roughness of Surface-3 was higher and consequently the density of DNA molecules was higher compared to Surface-2. As a result fluorescence intensity was highest for Surface-3.

3.5. Isolation of hGBM and astrocyte cells on aptamer functionalized substrates

The aptamer used has been already established to selectively bind to overexpressed EGFR on tumor cells. The random/mutant sequences have been used in the past as control that showed no affinity for EGFR. Figures 4(A)–(D) show representative micrographs of hGBM cells captured on plain and nanotextured PDMS substrates functionalized with anti-EGFR aptamers. Average densities of hGBM and astrocyte cells were measured after washing the substrates with 1X PBS at 90 revolutions per minute for 15 min. The quantitative cell

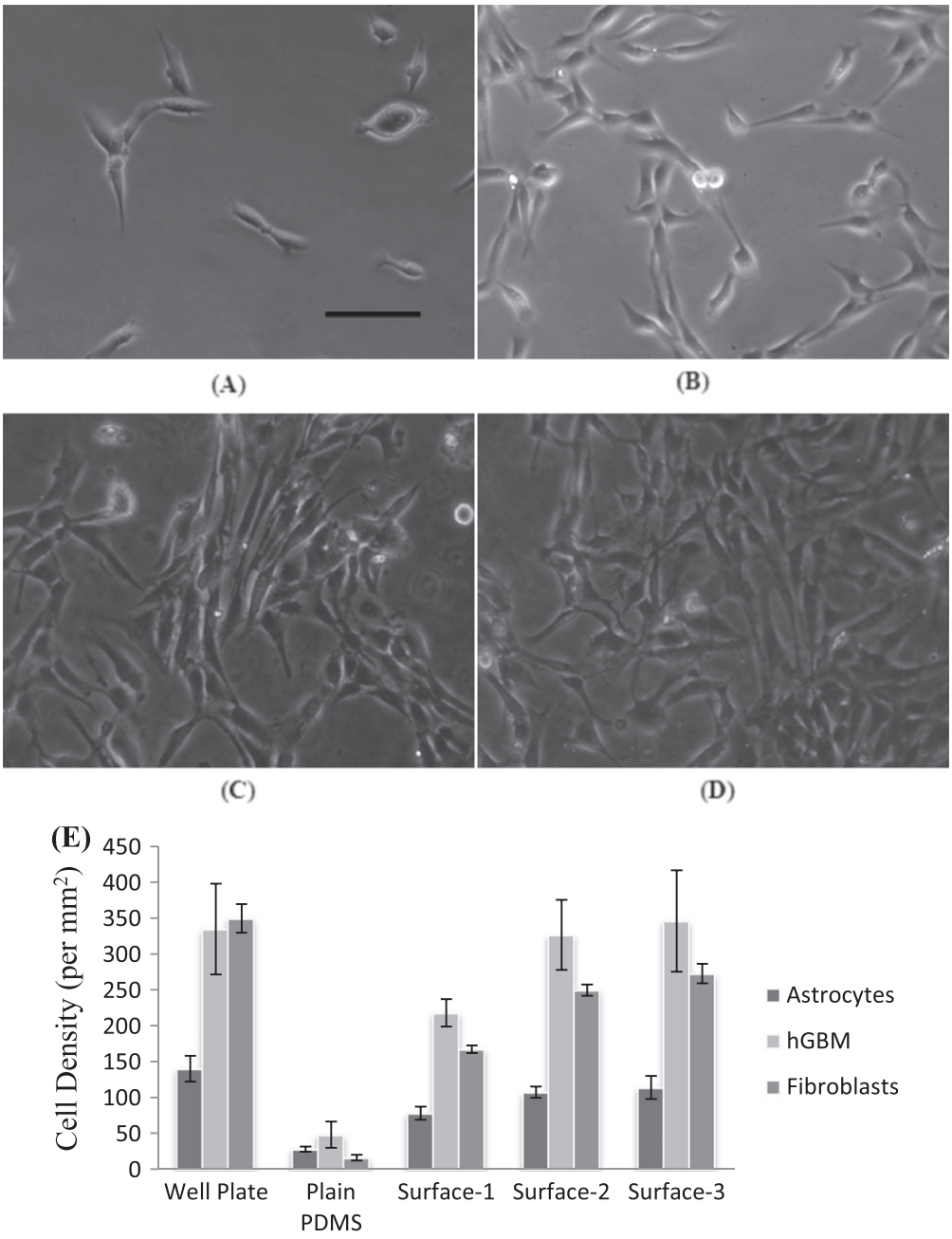

Figure 5. The hGBM cell growth on (A) plain PDMS surface; (B) Surface-1, (C) Surface-2 and (D) Surface-3; and (E) the average cell densities (cell number mm^{-2}) for hGBM, astrocyte and fibroblast cells on all surfaces. For hGBM cells, the growth is not statistically different between well plate, Surface-2 and Surface-3 (p-value >0.05) but these surfaces have statistically different cell density compared to plain PDMS and Surface-1 ($n = 6$). For astrocytes and fibroblast cells, the growth is statistically different among all the surfaces only except Surface-2 and Surface-3 (p-value >0.05). Scale bar = 100 μm in (A) is also applicable for (B)–(D).

density counts are shown in figure 4(E). By analyzing the optical micrographs of substrates it was found that the average number of captured hGBM cells was lower on plain PDMS compared to nanotextured PDMS surfaces. The average cell density for plain PDMS surface was 49.25 ± 7.21 per mm^2 and for Surface-1, -2 and -3 cell densities were 103.75 ± 5.28, 146.75 ± 5.50, and 166.38 ± 7.19 per mm^2, respectively (figure 4E). From the cell density on surfaces, the cell capture efficiency calculated for plain PDMS surface was only 9.85% whereas for Surface-3, it increased to 33.28%. Average cell densities of astrocyte cells did not vary significantly for all of these surfaces (figure 4E). For plain PDMS, cell density was 28 ± 9.80 mm^2 and for Surface-1, -2 and -3 these were 36 ± 15.18, 38 ± 14.03, and 44 ± 14.53 mm^2, respectively. Density of hGBM cells depended on the available number of anti-EGFR aptamer molecules on the substrate, the density of EGFR on cell membrane, the affinity between EGFR and aptamer, and the surface roughness of the substrate [16].

Nanotexture not only increased the availability of aptamer molecules on the surfaces, but it also increased the affinity between the surfaces and cells by offering a biomimetic

environment. Recent works have shown that basement membrane provides a nanotextured environment for cell support and possibly added focal points for metastatic cells to pass through the membrane and to get into the bloodstream [31]. Consequently, cell capture density was also improved. It can be observed thus that cell capture density was a direct function of surface nanotexturing. An almost linear correlation was found between surface roughness and tumor cell capture density when the data from the three nanotextured surfaces was compared. The higher the surface roughness was at nanoscale, the greater was the cell capture density. Both surface roughness and cell capture density of tumor cells were highest for Surface-3 and lowest for Surface-1. Statistical analysis and one-way ANOVA showed statistically significant differences (p-value <0.01) in cell density for three surfaces.

For astrocyte cells, though densities of captured cells were slightly higher on nanotextured PDMS compared to plain surface, the differences were not as high as for tumor cells. Moreover, from figure 4(E), it is clearly visible that captured astrocyte cells were noticeably fewer on nanotextured PDMS relative to the hGBM cells. The functionalized nanotextured surfaces had a very high number of available aptamers, thus reducing the non-specific binding of astrocyte cells on the surfaces. These observations showed the essential trade-off between sensitivity and selectivity. On the whole, the nanotextured surfaces offered elevated sensitivity but these also suffered from lower specificity. The end-goal would define optimal levels of nanotexturing for particular applications against various cancers but here we can see that the nanotextured surfaces are advantageous to increase isolation of rare cancer cells. The data also alludes to the fact that for one type of tumor cells, with one level of receptor overexpression, the isolation efficiency could be increased by simply increasing the number of available ligands. Nanotexture on the PDMS substrates provides a simple and straight-forward way to implement that in microfluidic channels.

3.6. In vitro cell growth on bare nanotextured surfaces

The three types of cells were seeded on four PDMS surfaces and standard polystyrene well plates after laminin coating. The cell growth was significantly higher on nanotextured surfaces compared to plain PDMS surface for all three types of cells (figure 5). In every case, Surface-3 exhibited highest cell density among the three nanotextured surfaces after three days. The density of astrocyte cells also increased to 114 ± 16.15 cells per mm^2 on Surface-3 whereas plain PDMS had 28 ± 3.58 cells per mm^2. The well plate had higher cell density compared to Surface-3. Similarly, density of fibroblasts cells was also higher in well plate (349.6 ± 20.12 cells per mm^2) compared to Surface-3 (272.80 ± 13.68 cells per mm^2). One-way ANOVA analysis showed statistically significant differences in all substrates for astrocyte and fibroblast cells except for astrocyte cells in Surface-2 and Surface-3. In this case, the cell density was not significantly different (p-value = 0.29). For hGBM cells, statistical differences among well plate, Surface-2 and Surface-3 was not substantial (p-value >0.39). For hGBM cells, nanotextured surfaces showed higher cell growth, which was very similar to the well plate.

A limitation of plain PDMS is that even after chemical functionalization, it is a challenge to maintain cells on surface, especially for long-term cell culture due to lack of stable cell-adhesive layer [16, 33]. The generated hydroxyl groups undergo dehydration reaction, and high chain mobility pulls the hydrophobic methyl groups to the surface and prohibits the formation of a cell-adhesive layer. The same would also occur on nanotextured PDMS surfaces but nanotexturing improves cell attachment and isolation by increasing surface area, which allows for more protein attachment and facilitates greater cell adhesion and growth. Thus, the nanotextured surfaces allowed higher cell growth. Especially for tumor cells, the growth was comparable to the standard well plate. But for healthy cells, the well plate had much higher cell growth compared to nanotextured surfaces. This analysis represented that tumor cells have higher affinity towards nanotextured surfaces compared to healthy cells. Consequently, nanotextured PDMS surface can be a fascinating feature in microfluidic platforms for isolation and growth of tumor cells as microfluidic devices can allow for similar growth as standard well plate material.

4. Conclusions

Approaches to synthesize nanotextured PDMS surfaces provide rapid and cost-effective ways of fabricating cell isolation and cell-culture substrates. By controlling the ratio of etchants and time of etching, different surface roughnesses were achieved. Nanotextured PDMS surfaces showed higher cell capture capability and allowed for faster cell growth compared to plain PDMS. The surface roughness influenced cell capture and cell growth almost linearly. Therefore, nanotextured PDMS could be implemented in biosensors, especially in microfluidic devices. The growth rate of the tumor cells was also higher on nanotextured PDMS surfaces than plain PDMS. This work can significantly enhance the cell culture capabilities of microfluidic devices.

Acknowledgments

The authors would like to acknowledge useful discussions and help from Azhar Ilyas, Waqas Ali, Nuzhat Mansur, Raja Raheel Khanzada and Mohammad Raziul Hassan. The work was supported by Cancer Research Foundation of North Texas. The tumor samples were provided by Dr Robert Bachoo from the University of Texas Southwestern Medical Center at Dallas. The aptamer molecules were provided by Dr. Andrew Ellington from the University of Texas at Austin.

References

[1] Adams A A, Okagbare P I, Feng J, Hupert M L, Patterson D, Gottert J, McCarley R L, Nikitopoulos D, Murphy M C and Soper S A 2008 Highly efficient circulating tumor cell isolation from whole blood and label-free enumeration using polymer-based microfluidics with an integrated conductivity sensor *J. Am. Chem. Soc.* **130** 8633–41

[2] Chen J, Li J and Sun Y 2012 Microfluidic approaches for cancer cell detection, characterization, and separation *Lab Chip* **12** 1753–67

[3] MacDonald M P, Neale S, Paterson L, Richies A, Dholakia K and Spalding G C 2003 Cell cytometry with a light touch: sorting microscopic matter with an optical lattice *J. Biol. Regulators Homeostatic Agents* **18** 200–5

[4] Swennenhuis J F, Tibbe A G J, Levink R, Sipkema R C J and Terstappen L W M M 2009 Characterization of circulating tumor cells by fluorescence *in situ* hybridization *Cytometry* A **75** 520–7

[5] Dharmasiri U, Witek M A, Adams A A and Soper S A 2010 Microsystems for the capture of low-abundance cells *Annu. Rev. Anal. Chem.* **3** 409–31

[6] Tan S J, Yobas L, Lee G Y H, Ong C N and Lim C T 2009 Microdevice for the isolation and enumeration of cancer cells from blood *Biomed. Microdevices* **11** 883–92

[7] Nagrath S, Sequist L V, Maheswaran S, Bell D W, Irimia D, Ulkus L, Smith M R, Kwak E L, Digumarthy S and Muzikansky A 2007 Isolation of rare circulating tumour cells in cancer patients by microchip technology *Nature* **450** 1235–9

[8] Yu M, Stott S, Toner M, Maheswaran S and Haber D A 2011 Circulating tumor cells: approaches to isolation and characterization *J. Cell Biol.* **192** 373–82

[9] Fischer N O, Tarasow T M and Tok J B H 2007 Aptasensors for biosecurity applications *Curr. Opin. Chem. Biol.* **11** 316–28

[10] Siegel R, Naishadham D and Jemal A 2012 Cancer statistics, 2012 *CA: Cancer J. Clinicians* **62** 10–29

[11] Curry S J, Byers T and Hewitt M 2003 *Fulfilling the Potential for Cancer Prevention and Early Detection* (Washington, DC: National Academy Press)

[12] Smith R A, Cokkinides V, von Eschenbach A C, Levin B, Cohen C, Runowicz C D, Sener S, Saslow D and Eyre H J 2002 American cancer society guidelines for the early detection of cancer *CA: Cancer J. Clinicians* **52** 8–22

[13] Toner M and Irimia D 2005 Blood-on-a-chip *Annu. Rev. Biomed. Eng.* **7** 77–103

[14] Xu Y, Phillips J A, Yan J, Li Q, Fan Z H and Tan W 2009 Aptamer-based microfluidic device for enrichment, sorting, and detection of multiple cancer cells *Anal. Chem.* **81** 7436–42

[15] Mahmood M, Wan Y, Islam M, Ali W, Hanif M, Kim Y-T and Iqbal S M 2014 Micro-nanotexturing of substrates to enhance ligand-assisted cancer cell isolation *Nanotechnology* **25** 475102

[16] Wan Y, Mahmood M, Li N, Allen P B, Kim Y-T, Bachoo R, Ellington A D and Iqbal S M 2012 Nanotextured substrates with immobilized aptamers for cancer cell isolation and cytology *Cancer* **118** 1145–54

[17] Bacakova L, Filova E, Parizek M, Ruml T and Svorcik V 2011 Modulation of cell adhesion, proliferation and differentiation on materials designed for body implants *Biotechnol. Adv.* **29** 739–67

[18] Asghar W, Kim Y-T, Ilyas A, Sankaran J, Wan Y and Iqbal S M 2012 Synthesis of nano-textured biocompatible scaffolds from chicken eggshells *Nanotechnology* **23** 475601

[19] Biela S A, Su Y, Spatz J P and Kemkemer R 2009 Different sensitivity of human endothelial cells, smooth muscle cells and fibroblasts to topography in the nano-micro range *Acta Biomater.* **5** 2460–6

[20] Thapa A, Miller D C, Webster T J and Haberstroh K M 2003 Nano-structured polymers enhance bladder smooth muscle cell function *Biomaterials* **24** 2915–26

[21] Miller D C, Thapa A, Haberstroh K M and Webster T J 2004 Endothelial and vascular smooth muscle cell function on poly (lactic-co-glycolic acid) with nano-structured surface features *Biomaterials* **25** 53–61

[22] Tsougeni K, Tserepi A, Boulousis G, Constantoudis V and Gogolides E 2007 Control of nanotexture and wetting properties of polydimethylsiloxane from very hydrophobic to super-hydrophobic by plasma processing *Plasma Process. Polym.* **4** 398–405

[23] Vlachopoulou M E, Petrou P S, Kakabakos S E, Tserepi A and Gogolides E 2008 High-aspect-ratio plasma-induced nanotextured poly (dimethylsiloxane) surfaces with enhanced protein adsorption capacity *J. Vac. Sci. Technol.* B **26** 2543–8

[24] Cheng M M-C, Cuda G, Bunimovich Y L, Gaspari M, Heath J R, Hill H D, Mirkin C A, Nijdam A J, Terracciano R and Thundat T 2006 Nanotechnologies for biomolecular detection and medical diagnostics *Curr. Opin. Chem. Biol.* **10** 11–9

[25] Soleymani L, Fang Z, Sargent E H and Kelley S O 2009 Programming the detection limits of biosensors through controlled nanostructuring *Nat. Nanotechnology* **4** 844–8

[26] Devabhaktuni S and Prasad S 2009 Nanotextured organic light emitting diode based chemical sensor *J. Nanoscience Nanotechnology* **9** 6299–306

[27] Dylewicz R, Khokhar A Z, Wasielewski R, Mazur P and Rahman F 2011 Nanotexturing of GaN light-emitting diode material through mask-less dry etching *Nanotechnology* **22** 055301

[28] Wan Y, Kim Y-T, Li N, Cho S K, Bachoo R, Ellington A D and Iqbal S M 2010 Surface-immobilized aptamers for cancer cell isolation and microscopic cytology *Cancer Res.* **70** 9371–80

[29] Park T H and Shuler M L 2003 Integration of cell culture and microfabrication technology *Biotechnol. Prog.* **19** 243–53

[30] Vlachopoulou M-E, Tserepi A, Petrou P S, Gogolides E and Kakabakos S E 2011 Protein arrays on high-surface-area plasma-nanotextured poly (dimethylsiloxane)-coated glass slides *Colloids Surf.* B **83** 270–6

[31] Hufnagel H, Huebner A, Gulch C, Guse K, Abell C and Hollfelder F 2009 An integrated cell culture lab on a chip: modular microdevices for cultivation of mammalian cells and delivery into microfluidic microdroplets *Lab Chip* **9** 1576–82

[32] Kohli P, Harrell C C, Cao Z, Gasparac R, Tan W and Martin C R 2004 DNA-functionalized nanotube membranes with single-base mismatch selectivity *Science* **305** 984–6

[33] Sankaran J S, Goyal S, Kahsai W T, Pham U H T and Iqbal S M 2011 Hydrophilic interfacing for thermal micro assembly of polymers (HITMAP) *Adv. Sci. Lett.* **4** 3464–9

[34] Yamazoe T *et al* 2013 A synthetic nanofibrillar matrix promotes *in vitro* hepatic differentiation of embryonic stem cells and induced pluripotent stem cells *J. Cell Sci.* **126** 5391–9